Applied Soft Computing 66 (2018) 413–427

Contents lists available at ScienceDirect

Applied Soft Computing

journal homepage: www.elsevier.com/locate/asoc

Image co-segmentation using dual active contours

Ashish Ghosh*, Sanmoy Bandyopadhyay

Center for Soft Computing Research, Indian Statistical Institute, Kolkata 700108, India

ARTICLE INFO

Article history:
Received 9 March 2016
Received in revised form 16 January 2018
Accepted 19 February 2018
Available online 23 February 2018

Keywords:
Co-segmentation
Active contour model
Chan–Vese active contour
Dual-geometric active contours
Inner contour
Outer contour
Gradient descent

ABSTRACT

In this article a novel algorithm is proposed to segment a pair of images simultaneously (co-segmentation) for extracting common objects. The task of co-segmentation has been performed using the dual geometric active contour model. Both the contours (of the objects) are initialized and evolved simultaneously in the given images. As the contours proceed towards the boundary of the common object(s) present in the images, energy value gets reduced. The contours are allowed to evolve until both the inner and the outer contours coincide at the object boundary. The resultant images formed are known as the co-segmented images. The proposed approach is evaluated on 20 benchmark datasets and compared with the state-of-the-art methods. Results show that the performance of the proposed method is better than the compared methods.

1. Introduction

Detection of similar regions (common object(s)) between images is an area of interest in the field of computer vision. The main idea behind detection of similarity between images is to establish a relation between the images. One of the ways of establishing similarities among the images is by detecting common object(s) in the images. The common object(s) detection has a wide range of applications, such as video object (common) detection [1,2], video summarization [3], image retrieval [3–6], creating visual summary of images or videos [7,8], recognition of people wearing the same clothes [9], detection of aircraft from high-resolution satellite images [10], medical applications like pathology detection in brain images [11], motor neuron morphology estimation in brain [12], biomedical imaging applications to identify small pathologies [13], automatic segmentation of abdominal organs [14].

To extract common objects from given images, a new method has been developed by Rother et al. [3]. The method termed as co-segmentation, is the task of simultaneously segmenting the common parts of an image pair. More specifically, to say, each image contains the "same" foreground object(s) in front of "changeable" backgrounds and in comparison to the single image segmentation case, the task is to carry out segmentation of the common object(s) simultaneously in all images [8]. Here segmentation of common object(s) is performed by incorporating the information of one image with other image(s). To extract common region (object(s)), it measures similarity between the two images by comparing the statistics of two images such as color histogram, texture, etc. The advantage of this method of common object(s) detection is that, it does not require any registration among objects present in the given images.

Many methodologies [3,11,13,15] have been developed for performing co-segmentation. Among them active contour model (ACM) based methods have several advantages. First, the objective function for active contour (AC) based co-segmentation is a convex optimization problem which can be solved in linear time, unlike the other existing co-segmentation methods. Second, the method does not depend on the accurate prior information of the object like MRF model for co-segmentation [3,11,13]. Third, the method does not require any accurate and exact human interaction to generate the co-segmented output. However, this AC based co-segmentation method uses level set formulation [15,16]. The level set formulation of ACM has an advantage that by changing the topology of level set function the contour can either split or merge [17]. This characteristic makes the level set function detect multiple boundaries in the images. However, it has a disadvantage. It usually searches minima in a local manner [15,18]. This, in turn, increases the rate of misinterpretation of regions and decreases the accuracy of co-segmentation. To overcome the aforementioned issue of ACM, dual-geometric active contour model (DGACM) based method, which shows promises [18–20] in case of single image seg-

* Corresponding author.
E-mail addresses: ash@isical.ac.in (A. Ghosh), sanmoy1985@rediffmail.com (S. Bandyopadhyay).

https://doi.org/10.1016/j.asoc.2018.02.034
1568-4946/

mentation, can be used. However, in its current form it cannot be applied for co-segmentation.

In this work a novel approach for co-segmentation using a new variant of DGACM has been proposed. The formulation of the energy function has been modified to tackle the problem of common object(s) extraction. The algorithm is applied over a pair of images, with two contours for each of the images. Outer contour is made to evolve on the boundary of the images circumscribing (enclosing) the object regions and the inner contour is made to evolve inside the object region near the center of the images. The outer is made to shrink towards the object boundary and the inner one is made to expand towards the object, and thus it has the ability to detect the boundary of common object(s) in the images. As a consequence, one of the challenges becomes to initialize the contour. In this work, a heuristic method has been proposed to initialize two contours on the input images without human intervention. In summary the main contribution in this article is as follows:

- The task of image co-segmentation has been performed using dual- geometric active contour model (DGACM).
- DGACM based segmentation has been re-formulated by incorporating the information sharing function between contours of different images.
- A heuristic approach to initialize both the inner contours is suggested.

Experiments have been conducted on 20 pairs of benchmark images. The error-rate of the proposed co-segmentation method has been taken into consideration to establish the effectiveness of the proposed model. Results of the proposed technique have been compared with those of other existing co-segmentation algorithms and single and dual-geometric active contour (DGAC) based image segmentation. It is seen that the proposed method is capable of producing better results as compared to those of the existing algorithms of co-segmentation.

The rest of the article is organized as follows. Section 2 describes the related work on image co-segmentation. The proposed work on co-segmentation using dual active contours has been presented along with other related methodologies in Section 3. In Section 4, detail analysis and comparison of results obtained using the proposed approach and other algorithms are presented. Finally, conclusion of the overall work and future direction of research are presented in Section 5.

2. Related work

In the literature, various techniques have been suggested for image co-segmentation to detect common object(s). In contrast to image segmentation [16,19,21–25], which deal with a single image and segment the image into a number of homogeneous parts, co-segmentation techniques deal with two or more images and segment out the common parts of the images. Many optimization (minimization) techniques have been used to have accurate image co-segmentation. Addition of foreground similarity terms, with the existing segmentation model, leads to the concepts of co-segmentation. The motive is to optimize (minimize) the co-segmentation energy function to get the common object(s) in the images. For this purpose both the local smoothness in each image and the foreground similarity between the images are taken into account [26].

Rother et al. [3] applied MRF model [27–29] for co-segmentation. They have introduced two terms from the traditional MRF. One represents deviation (or data) penalty, charged for a pixel set in the foreground, although there is a-priori information indicating they should be in the background. Another represents separation or smoothness penalty, which measures the cost of assigning different labels to two neighboring pixels [11]. Along with these two terms another term, the global energy term, has also been introduced to encode similarity among the foreground histograms of both the images. The total energy equation changes based on the assertion of the global energy term. In Rother et al.'s [3] model for co-segmentation, histogram similarity is computed between the foreground of the images based on $L1-norm$. However $L1-norm$ is not differentiable due to which the optimization problem becomes complex. In order to overcome this drawback, Mukherjee et al. [13] introduced $L2-norm$, where they have used the squared Euclidean distance for measuring the global energy. Both $L1-norm$ and $L2-norm$ models of co-segmentation, lead to NP-hard optimization problem [3,8,13].

To overcome the shortcoming of these models, Hochbaum and Singh [11] proposed a reward model in global energy term in place of penalty term. However, this reward method also leads to a submodular optimization problem in co-segmentation. Moreover, in the reward based method the accuracy of co-segmentation depends on the precise object prior to building the unary term of the energy function for which it requires human interaction to initialize common objects' locations. Vicente et al. in [8] incorporated, modified Boykov–Jolly model [30] in the global energy term as the foreground similarity measurement, and in the MRF model only the smoothness penalty has been incorporated. In these co-segmentation methods, the common objects are assumed to contain similar colors [31]. Merdassi et al. [32] put forward the concept of Fuzzy – MRF model in co-segmentation, where a fuzzy classification technique has been proposed in order to eliminate the ambiguity of a pixel membership to a histogram bin, especially for pixels on bins' borders.

Apart from these MRF based methods of co-segmentation there are several other methods which have been employed for co-segmentation. A clustering based method has been proposed by Joulin et al. [33]. They have introduced discriminative clustering technique to train the supervised classifier by labeling the foreground and background pixels in all the images jointly in order to maximize the differences between the common object(s) and the background in the images [34]. This idea of discriminative clustering based co-segmentation method was extended to present a multi-class co-segmentation method to segment the common objects of multiple images [35]. Hierarchical image clustering has also been developed for the purpose of co-segmentation [36]. Here, the authors first used a clustering technique to perform segmentation of the given images. Then inter and intra image connection was developed based upon clustering method for detection of common object(s). A method of co-segmentation by composition has been developed in [37]. In this work, co-segmentation has been initialized by inducing affinities between the image parts. The main drawback of this method is that, it fails to detect small parts of common object(s) in images [37]. Dai et al. [38] has introduced unsupervised learning based framework for performing co-segmentation, where co-sketch of the image has been applied to align foreground objects. Another method of image co-segmentation have been proposed by Jerripothula et al. [39]. In this paper, the task of co-segmentation have been carried out using saliency co-fusion. However, the method has limitation in case of improper saliency maps and images containing similar background [39]. In the paper [40], the common object from the images have been detected using a coupling of two methods, namely: co-segmentation and co-skeletonization. The reason behind this method of common object detection is to share well defined information from each of the methods to produce better output. Although, the method has to depend on quality of neighboring images for proper salient features [40]. Moreover the method shows its limitations for images containing objects at

different viewpoints or of different sizes [40]. An unsupervised model of co-segmentation has been introduced by Li et al. [41] for multiple common foreground objects detection, using the object proposal selection technique. As a consequence the accuracy of the co-segmentation output depends on the proper generation of the proposal [41]. An interactive co-segmentation approach has also been proposed by Wang et al. [42] using higher-oder energy optimization technique and likelihood estimation. Its performance depends on proper computation of the prior knowledge using likelihood estimation method.

In addition to these methods there are other methods/models which have been applied for solving the co-segmentation problem. These are random walk segmentation methods [43], interactive co-segmentation model [44], heat diffusion method [45] etc. Recently Meng et al. [15] used the ACM to extract out the common object(s) from the given images. They have used the level set (region based) to formulate energy function of ACM. Here the color rewarding strategy has been used to measure the foreground similarity, which makes the energy function easy for optimization. In addition, a rewarding strategy has been implemented for both the foreground reward and the background reward, in order to measure the foreground similarity and background consistency. In this process, a mutual evolutionary approach has been applied to minimize the energy function.

3. Proposed work of co-segmentation using dual active contours

Although, single active contour model (SACM) based co-segmentation [15] provide outputs with lower error-rate as compared to other existing algorithms, it suffers from the tendency to getting stuck to the local minima [15,18,21,46]. As a result, sometimes improper object boundary is detected, which in turn increases the error-rate of common object(s) detection. As a result, there is a chance of misclassification, i.e. some pixels are classified as the foreground, although there is a prior information that it should be in the background. These small regions are caused by the topology changes of the level sets. Minimization of this topological change of the level set may reduce the efficacy of the method for co-segmentation to control the variations, e.g. shape and pose among the common object(s). A post-processing has been applied to remove the small regions without limiting the topological changes of the level set. But this process is not sufficient to carry away the entire small regions or correct the misclassification of regions or pixels, especially for those regions which are connected with the foreground regions [15]. This is due to the fact that level sets used for minimizing the energy function, searches the minimum locally. The global optimization search has been applied in some work related to co-segmentation such as [11], but its accuracy depends on the user interaction.

3.1. Classical dual-geometric active contours for segmentation

In general SACM energy function stuck at local minima values corresponding to the strong edges (not necessarily edges of the desired object(s)) or false boundaries. In this situation the contour may get trapped in strong neighbouring edges resulting in false boundary detection [18,47]. As a result, there is a chance that some of the background pixels are misinterpreted as foreground pixels. To avoid this problem and to reduce misclassification of pixels, in this work a novel approach for co-segmentation have been proposed. In this work DGACM have been accomplished as a novel technique for performing the task of co-segmentation. The dual-parametric active contour method (DPACM) for single image segmentation was proposed by Gunn and Nixon [18]. Here the two contours, inner and outer, are generated simultaneously. The outer is made to contract towards the object boundary and the inner is made to expand towards it. It has the advantage that it searches the minimum of the energy function in a global manner, and thus reduces misclassification of pixels in the images [18–20]. Based on the work of Gunn and Nixon [18], DGAC was implemented on Chan–Vese (C–V) model [16] for single image segmentation by Zhu et al. [19] and by Huang et al. [20]. The energy function for DGACM based segmentation given in [19,20] as follows:

$$E^{*}_{DCV}(\Phi,\Psi) = E_{CV}(\Phi)+E_{CV}(\Psi) + \tau\int_{\Omega}[H(\Phi(x,y))-H(\Psi(x,y))]^{2}dxdy. \quad (1)$$

The first term on the right-hand-side of Eq. (1) indicates the energy function of the outer curve and second term denotes the energy function of the inner contour given by the Chan–Vese active contour model (C-VACM) [16]. The last term on the right-hand-side of Eq. (1) is incorporated to alleviate the difference between the inner and the outer contours and τ denotes the weight parameter for the interaction term.

$$\Phi(x,y) \;\; or \;\; \Psi(x,y) = \begin{cases} > 0 : \text{if } (x,y) \text{ is inside } C, \\ = 0 : \text{if } (x,y) \text{ is on } C, \\ < 0 : \text{if } (x,y) \text{ is outside } C; \end{cases} \quad (2)$$

where the contour C can be represented as shown in Eq. (3):

$$C = \begin{cases} \{(x,y)|\Phi(x,y)=0\}, & \text{for outer contour} \\ \text{or} & \\ \{(x,y)|\Psi(x,y)=0\}, & \text{for inner contour.} \end{cases} \quad (3)$$

Now based on Chan–Vese active contour model (C-VACM) [16] it can be stated that, in Eq. (1),

$$E^{*}_{CV}(\Phi) = \mu Length(C)+\nu Area(C^{i}) + \lambda_1\int_{C^{i}} f[I(x,y),u_1]dxdy+\lambda_2\int_{C^{o}} f[I(x,y),u_2]dxdy. \quad (4)$$

The level set formulation of C-VACM energy function [16] given in Eq. (4) can be expressed as

$$E^{*}_{CV}(\Phi) = \mu\int_{\Omega}\delta(\Phi(x,y))|\nabla(\Phi(x,y))|dxdy+\nu\int_{\Omega}H(\Phi(x,y))dxdy + \lambda_1\int_{\Omega} f[I(x,y),u_1]H(\Phi(x,y))dxdy + \lambda_2\int_{\Omega} f[I(x,y),u_2](1-H(\Phi(x,y)))dxdy; \quad (5)$$

where

$$f[I(x,y),u_1] = |I(x,y)-u_1|^{2}; \quad (6)$$

and

$$f[I(x,y),u_2] = |I(x,y)-u_2|^{2}. \quad (7)$$

In Eqs. (6) and (7), the terms u_1 and u_2 denote the mean intensity of the pixels inside and outside the outer curve respectively [16]. Similarly, the energy function for the inner contour $E_{CV}(\Psi)$ can be represented as,

$$E^{*}_{CV}(\Psi) = \mu\int_{\Omega}\delta(\Psi(x,y))|\nabla(\Psi(x,y))|dxdy+\nu\int_{\Omega}H(\Psi(x,y))dxdy + \lambda_1\int_{\Omega} f[I(x,y),v_1]H(\Psi(x,y))dxdy + \lambda_2\int_{\Omega} f[I(x,y),v_2](1-H(\Psi(x,y)))dxdy; \quad (8)$$

where, the terms v_1 and v_2 indicate the mean intensity of the pixels inside and outside the inner curve respectively [16].

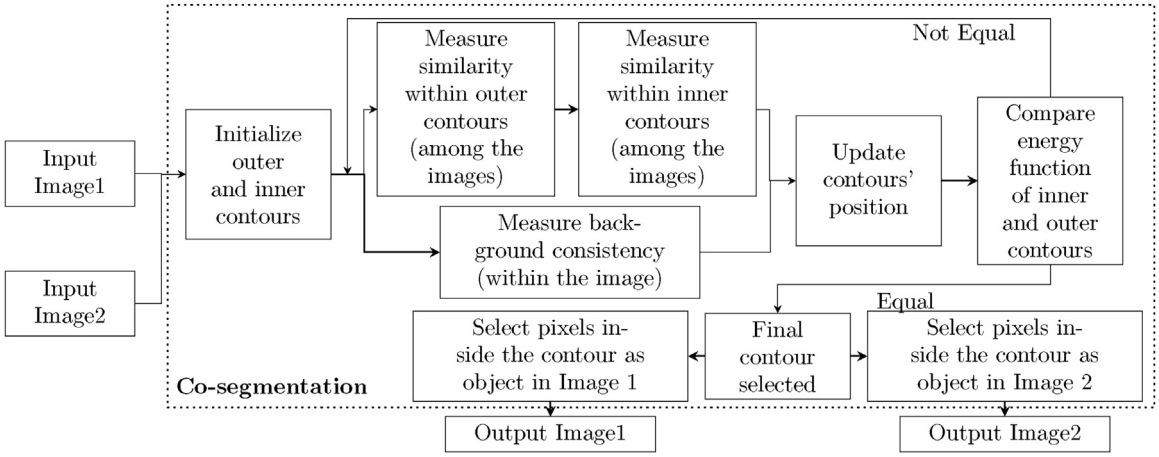

Fig. 1. Block-diagram of the proposed method.

Thus, based on Eqs. (5) and (8), Eq. (1) can be rewritten as:

$$
\begin{aligned}
E^{*}_{DCV}(\Phi,\Psi) &= \mu\int_{\Omega}\delta(\Phi(x,y))|\nabla(\Phi(x,y))|dxdy+\nu\int_{\Omega}H(\Phi(x,y))dxdy\\
&+\lambda_1\int_{\Omega}f[I(x,y),u_1]H(\Phi(x,y))dxdy+\lambda_2\int_{\Omega}f[I(x,y),u_2](1-H(\Phi(x,y)))dxdy\\
&+\mu\int_{\Omega}\delta(\Psi(x,y))|\nabla(\Psi(x,y))|dxdy+\nu\int_{\Omega}H(\Psi(x,y))dxdy\\
&+\lambda_1\int_{\Omega}f[I(x,y),v_1]H(\Psi(x,y))dxdy+\lambda_2\int_{\Omega}f[I(x,y),v_2](1-H(\Psi(x,y)))dxdy\\
&+\tau\int_{\Omega}[H(\Phi(x,y))-H(\Psi(x,y))]^2dxdy,
\end{aligned}
\tag{9}
$$

which is the overall energy function for DGACM based segmentation.

3.2. Formulation of dual-geometric active contours for co-segmentation

The exchange of pixels information between the images is the backbone of the image co-segmentation task, since, the main motivation of the image co-segmentation is to extract out the common object(s) from the images. As such the classical contour based method of segmentation [16,19,20] fail for the mentioned purpose. The main cause behind this claim is that the formulation of sharing information between the images does not feature in the theory of classical contour based method of segmentation. The terms u_1 and u_2 are only capable to deal with the pixels present within the image to be segmented. This also holds true for the case of v_1 and v_2, the terms associated with inner contour, in case of DGACM based segmentation. Thus, in order to achieve the goal of co-segmentation, the terms u_1 and u_2 present in classical DGACM have been replaced by the notion of $r(C^i_{1-k})$ and $r(C^o_k)$ respectively. As a consequence the functions $f[I(x,y),u_1]$ and $f[I(x,y),u_2]$ have been replaced by the terms $f[I_k(x,y),r(C^i_{1-k})]$ and $f[I_k(x,y),r(C^0_k)]$ respectively, as stated in [15]. Basically the term $f[I_k(x,y),r(C^i_{1-k})]$ play key factors for exchanging the information between the images in the task of co-segmentation. Thus, the re-formulated level set formulation of C-VACM energy function [16] stated in Eq. (5), can be expressed as given in Eq. (10) [15]. In the similar manner, this hold true for the case of v_1 and v_2. The re-formulated equation for the inner contour is given in Eq. (11).

In the proposed DGACM based co-segmentation method, two contours are initialized simultaneously in each of the images, outer contours near the boundary of both the images, and the inner contours inside the images. The initial contours set-up for co-segmentation using SACM and the proposed method are shown in Fig. 2 for comparison. The outer contour is made to shrink towards the common foreground boundary and the inner is made to expand towards the same. Basically, the SACM has tendency to stick at local minima, as stated earlier. Now addition of extra contour with the existing SACM will provide extra force. That is, the function $H(\Psi(x,y))$ of the inner contour, in equation $\tau\int_{\Omega}[H(\Phi(x,y))-H(\Psi(x,y))]^2$, based on the pixels information present inside and outside the contour, act as a extra pulling force, and pulls the outer contour towards itself. This also holds true for the case of outer contour, where the function $H(\Phi(x,y))$ of the outer contour pull the inner contour towards itself. Thus, it avoids getting the contours trapped to local minima and as a result the chance of misclassification of pixels gets reduced. It can be stated that the energy function and the extra pulling force are based on the pixels information associated with each of the contours. Thus, through this process it incorporates the information among two contours (inner and outer), and as a result it overcomes the drawbacks of standard co-segmentation using SACM. Basically the function $\tau\int_{\Omega}[H(\Phi(x,y))-H(\Psi(x,y))]^2$ act as a coupling term between two contours (inner and outer). Block-diagram of the proposed work is shown in Fig. 1.

The energy function (for co-segmentation) of the outer curve [15] is formulated as:

$$
\begin{aligned}
E^{*}_{coseg}(\Phi) &= \mu\int_{\Omega}\delta(\Phi(x,y))|\nabla(\Phi(x,y))|dxdy+\nu\int_{\Omega}H(\Phi(x,y))dxdy\\
&-\lambda^i_k\int_{\Omega}f[I_k(x,y),r\left(C^i_{1-k}\right)]H(\Phi(x,y))dxdy\\
&-\lambda^o_k\int_{\Omega}f[I_k(x,y),r\left(C^o_k\right)](1-H(\Phi(x,y)))dxdy;
\end{aligned}
\tag{10}
$$

and the energy function of the inner contour is formulated as:

$$
\begin{aligned}
E^{*}_{coseg}(\Psi) &= \mu\int_{\Omega}\delta(\Psi(x,y))|\nabla(\Psi(x,y))|dxdy+\nu\int_{\Omega}H(\Psi(x,y))dxdy\\
&-\lambda^i_k\int_{\Omega}f[I_k(x,y),r\left(C^i_{1-k}\right)]H(\Psi(x,y))dxdy\\
&-\lambda^o_k\int_{\Omega}f[I_k(x,y),r\left(C^o_k\right)](1-H(\Psi(x,y)))dxdy.
\end{aligned}
\tag{11}
$$

The total energy function for the proposed DGACM for co-segmentation model is formulated as in Eq. (1). Here $E^{*}_{CV}(\Phi)$ and $E^{*}_{CV}(\Psi)$ have been replaced with equations $E^{*}_{coseg}(\Phi)$ and $E^{*}_{coseg}(\Psi)$

(a) (b) (c) (d)

Fig. 2. The initial contour set-up using single ACM are shown in (a) and (b), and using the proposed method are shown in (c) and (d).

respectively. Thus the overall energy function for the curve takes the form:

$$\begin{aligned} E^*_{dcoseg}(\Phi,\Psi) &= \mu\int_\Omega \delta(\Phi(x,y))|\nabla(\Phi(x,y))|dxdy + \nu\int_\Omega H(\Phi(x,y))dxdy \\ &-\lambda^i_{\Phi k}\int_\Omega f[I_k(x,y), r_\Phi\left(C^i_{1-k}\right)]H(\Phi(x,y))dxdy \\ &-\lambda^o_{\Phi k}\int_\Omega f[I_k(x,y), r_\Phi\left(C^o_k\right)](1-H(\Phi(x,y)))dxdy \\ &+\mu\int_\Omega \delta(\Psi(x,y))|\nabla(\Psi(x,y))|dxdy + \nu\int_\Omega H(\Psi(x,y))dxdy \\ &-\lambda^i_{\Psi k}\int_\Omega f[I_k(x,y), r_\Psi\left(C^i_{1-k}\right)]H(\Psi(x,y))dxdy \\ &-\lambda^o_{\Psi k}\int_\Omega f[I_k(x,y), r_\Psi\left(C^o_k\right)](1-H(\Psi(x,y)))dxdy \\ &+\tau\int_\Omega [H(\Phi(x,y)) - H(\Psi(x,y))]^2 dxdy. \end{aligned} \tag{12}$$

where k denotes the number of images.

For our simulation $k=0$, and 1. Term, $I(x,y)$ denotes the image pixel intensity at co-ordinate point (x,y). The term $\mu>0$ is a weight parameter given to the length of the curve, which depends on the number and size of the object(s) to be detected. The parameter $\nu>0$ is the weight given to the total area inside the curve, which allow to push the curve towards the object(s). The term $f[I_k(x,y), r_\Phi(C^i_{1-k})]$ measures the similarity between pixels inside the outer curve of both the images. Measure of similarity between pixels belonging to regions inside and outside of the outer curve of the same image is given by $f[I_k(x,y), r_\Phi(C^o_k)]$. The term $f[I_k(x,y), r_\Psi(C^i_{1-k})]$ is used to measure the similarity between pixels inside the inner curve of the images. The similarity measure between the pixels present inside and outside the inner curve within the same image is given by $f[I_k(x,y), r_\Psi(C^o_k)]$. The terms $f[I_k(x,y), r_\Phi(C^i_{1-k})]$ and $f[I_k(x,y), r_\Psi(C^i_{1-k})]$ which determine the similarity between the foreground image pixels and the region inside the curve of other image, are based on the color reward strategy. Here basically the pixels with similar color are rewarded with value "1", if not "0". The terms $r_\Phi(C^i_{1-k})$ and $r_\Psi(C^i_{1-k})$ denote the regions inside the outer and the inner curves of associated images, respectively. The region outside the bounds of the outer and the inner curves are represented by $r_\Phi(C^o_k)$ and $r_\Psi(C^o_k)$, respectively. The term $\lambda^i_{\Phi k}$ and $\lambda^o_{\Phi k}$ are the weight parameters used for the outer contour, while $\lambda^i_{\Psi k}$ and $\lambda^o_{\Psi k}$ are the weight parameters for the inner contour. The weight values $\lambda^i_{\Phi k}$ and $\lambda^i_{\Psi k}$ are used to maintain the uniformity among the common foreground pixels (pixels inside the contours) of the images. The terms $\lambda^o_{\Phi k}$ and $\lambda^o_{\Psi k}$ maintain the uniformity in the background of the image (measure similarity between pixels inside and outside of the contours within the images). The term Ω represents the regions of the image, $|\nabla(\Phi(x,y))|$ and $|\nabla(\Psi(x,y))|$ represent the gradient of inner and outer curve at the co-ordinate point (x,y) respectively, and $H(\Phi)$ represents the Heaviside (unit step) function [48]:

$$H(\Phi) = \begin{cases} 1, \text{ if } & \Phi \geq 0 \\ 0, \text{ if } & \Phi < 0; \end{cases} \tag{13}$$

and $\delta(\Phi)$ represents the Dirac measure (impulse function) [48] defined by

$$\delta(\Phi) = \frac{d(H(\Phi))}{d\Phi}. \tag{14}$$

Similarly, it holds true for the case of $H(\Psi)$ and $\delta(\Psi)$.

Now the goal is to generate the contour so that it can detect the common object(s) boundary by minimizing the energy function defined in Eq. (12). Thus, in order to evolve new level set function for the curves near the feature boundary, partial differential equation (PDE) is used. To minimize the energy function given by Eq. (12), gradient descent technique is applied on the corresponding Euler–Lagrange equation [49] of the defined energy function. The equivalent Euler–Lagrangian equation of the energy function given by Eq. (15) is:

$$\begin{aligned} &\frac{\partial(E^*_{dcoseg}(\Phi,\Psi))}{\partial\Phi} = -\mu\cdot\delta(\Phi)\text{div}\left(\frac{\nabla(\Phi)}{|\nabla(\Phi)|}\right) + \nu\cdot\delta(\Phi) \\ &-\lambda^i_{\Phi k}\cdot\frac{\partial f}{\partial\Phi}H(\Phi) - \lambda^i_{\Phi k}\cdot\delta(\Phi)f[I_k(x,y), r_\Phi\left(C^i_{1-k}\right)] \\ &-\lambda^o_{\Phi k}\cdot\frac{\partial f}{\partial\Phi}(1-H(\Phi)) + \lambda^o_{\Phi k}\cdot\delta(\Phi)f[I_k(x,y), r_\Phi\left(C^o_k\right)] \\ &+2\tau[H(\Phi(x,y)) - H(\Psi(x,y))]\delta(\Phi) = 0. \end{aligned} \tag{15}$$

The partial derivative $\frac{\partial f}{\partial\Phi} = 0$, as the functions $f[I_k(x,y), r_\Phi(C^i_{1-k})]$ and $f[I_k(x,y), r_\Phi(C^o_k)]$ are independent of Φ. Thus Eq. (15) can be rewritten as:

$$\begin{aligned} &\frac{\partial(E^*_{dcoseg}(\Phi,\Psi))}{\partial\Phi} = -\mu\cdot\delta(\Phi)\text{div}\left(\frac{\nabla(\Phi)}{|\nabla(\Phi)|}\right) + \nu\cdot\delta(\Phi) \\ &-\lambda^i_{\Phi k}\cdot\delta(\Phi)f[I_k(x,y), r_\Phi\left(C^i_{1-k}\right)] + \lambda^o_{\Phi k}\cdot\delta(\Phi)f[I_k(x,y), r_\Phi\left(C^o_k\right)] \\ &+2\tau[H(\Phi(x,y)) - H(\Psi(x,y))]\delta(\Phi) = 0. \end{aligned} \tag{16}$$

Similar to Eq. (16), by differentiating the energy function $E^*_{dcoseg}(\Phi,\Psi)$ with-respect-to Ψ, Eq. (17) is obtained as:

$$\begin{aligned} &\frac{\partial(E^*_{dcoseg}(\Phi,\Psi))}{\partial\Psi} = -\mu\cdot\delta(\Psi)\text{div}\left(\frac{\nabla(\Psi)}{|\nabla(\Psi)|}\right) + \nu\cdot\delta(\Psi) \\ &-\lambda^i_{\Psi k}\cdot\delta(\Psi)f[I_k(x,y), r_\Psi\left(C^i_{1-k}\right)] + \lambda^o_{\Psi k}\cdot\delta(\Psi)f[I_k(x,y), r_\Psi\left(C^o_k\right)] \\ &+2\tau[H(\Psi(x,y)) - H(\Phi(x,y))]\delta(\Psi) = 0. \end{aligned} \tag{17}$$

As a sequel, two associated Euler–Lagrange equation have been obtained, each for outer (Φ) and inner (Ψ) contours. Now perform-

ing the gradient descent on the obtained Euler–Lagrange equation [50], following equation is obtained:

$$\frac{\partial \Phi}{\partial t} = -\frac{\partial E(\Phi)}{\partial \Phi}. \tag{18}$$

Eqs. (16) and (17) can be reformulated as shown in Eqs. (19) and (20) respectively;

$$\begin{aligned}\frac{\partial \Phi}{\partial t} &= \delta(\Phi)\left\{\mu \cdot \mathrm{div}\left(\frac{\nabla(\Phi)}{|\nabla(\Phi)|}\right) - \nu + \lambda^{i}_{\Phi k} \cdot f[I_k(x,y), r_{\Phi}\left(C^{i}_{1-k}\right)]\right.\\ &\left. -\lambda^{o}_{\Phi k} \cdot f[I_k(x,y), r_{\Phi}\left(C^{o}_{k}\right)] - 2\tau[H(\Phi(x,y)) - H(\Psi(x,y))]\right\}\\ &= 0.\end{aligned} \tag{19}$$

$$\begin{aligned}\frac{\partial \Psi}{\partial t} &= \delta(\Psi)\left\{\mu \cdot \mathrm{div}\left(\frac{\nabla(\Psi)}{|\nabla(\Psi)|}\right) - \nu + \lambda^{i}_{\Psi k} \cdot f[I_k(x,y), r_{\Psi}\left(C^{i}_{1-k}\right)]\right.\\ &\left. -\lambda^{o}_{\Psi k} \cdot f[I_k(x,y), r_{\Psi}\left(C^{o}_{k}\right)] - 2\tau[H(\Psi(x,y)) - H(\Phi(x,y))]\right\}\\ &= 0.\end{aligned} \tag{20}$$

More elaborately, Eq. (19) can be written as:

$$\begin{aligned}\frac{\Phi^{t+1}_{k}(x,y) - \Phi^{t}_{k}(x,y)}{\Delta t} &= \delta(\Phi)\left\{\mu \cdot \mathrm{div}\left(\frac{\nabla(\Phi)}{|\nabla(\Phi)|}\right) - \nu\right.\\ &+\lambda^{i}_{\Phi k} f[I_k(x,y), r_{\Phi}\left(C^{i}_{1-k}\right)] - \lambda^{o}_{\Phi k} f[I_k(x,y), r_{\Phi}\left(C^{o}_{k}\right)]\\ &\left. -2\tau[H(\Phi(x,y)) - H(\Psi(x,y))]\right\} = 0,\end{aligned} \tag{21}$$

where $\Phi^{t}_{k}(x,y)$ denotes the outer curve evolved on the image during t^{th} iteration. Now assuming $\Delta t = 1$, the PDE of the evolving outer curve can be computed as shown in Eq. (22):

$$\begin{aligned}\Phi^{t+1}_{k}(x,y) &= \Phi^{t}_{k}(x,y) + \delta(\Phi)\left\{\mu \cdot \mathrm{div}\left(\frac{\nabla(\Phi)}{|\nabla(\Phi)|}\right) - \nu\right.\\ &+\lambda^{i}_{\Phi k} \cdot f[I_k(x,y), r_{\Phi}\left(C^{i}_{1-k}\right)] - \lambda^{o}_{\Phi k} \cdot f[I_k(x,y), r_{\Phi}\left(C^{o}_{k}\right)]\\ &\left. -2\tau[H(\Phi(x,y)) - H(\Psi(x,y))]\right\}.\end{aligned} \tag{22}$$

Similarly, the PDE of the evolving inner curve can be formulated as:

$$\begin{aligned}\Psi^{t+1}_{k}(x,y) &= \Psi^{t}_{k}(x,y) + \delta(\Psi)\left\{\mu \cdot \mathrm{div}\left(\frac{\nabla(\Psi)}{|\nabla(\Psi)|}\right) - \nu\right.\\ &+\lambda^{i}_{\Psi k} \cdot f[I_k(x,y), r_{\Psi}\left(C^{i}_{1-k}\right)] - \lambda^{o}_{\Psi k} \cdot f[I_k(x,y), r_{\Psi}\left(C^{o}_{k}\right)]\\ &\left. -2\tau[H(\Psi(x,y)) - H(\Phi(x,y))]\right\}.\end{aligned} \tag{23}$$

Eqs. (22) and (23) are used for minimization of the energy function and to evolve the new curves, i.e. outer and inner contours for both the images. Similar to the work done by Meng et al. in [15], the dynamic method for calculating $r_{\Phi}(C^{i}_{1-k})$ and $r_{\Psi}(C^{i}_{1-k})$ have also been applied. The overall steps of the proposed technique are given in Algorithm 1.

Algorithm 1. Proposed method.

1: $\Phi^{0}_{k} = 0$ Initialization: , , k = 0, 1, t = 0, and other parameters
2: $temp\_\Phi^{t}_{k} \longleftarrow \Phi^{0}_{k}$
3: $temp\_\Psi^{t}_{k} \longleftarrow \Psi^{0}_{k}$
4: **for** $n \leq maxiteration$ **do**
5: Calculate $r_{\Phi}(C^{i}_{1-k})$, $r_{\Phi}(C^{o}_{k})$, $r_{\Psi}(C^{i}_{1-k})$, and $r_{\Psi}(C^{o}_{k})$ for each image I_k
6: Calculate Φ^{t+1}_{k} solving PDE in $temp\_\Phi^{t}_{k}$ using Eq. (22)
7: Calculate Ψ^{t+1}_{k} solving PDE in $temp\_\Psi^{t}_{k}$ using Eq. (23)
8: **if** $(\Phi^{t+1}_{k} = \Psi^{t+1}_{k}$ & $\Phi^{t+1}_{k} = temp\_\Phi^{t}_{k}$ & $\Psi^{t+1}_{k} = temp\_\Psi^{t}_{k})||$ $(t = maxiteration)$ **then**
9: **goto** *Step 16.*
10: **break**;
11: **else**
12: $temp\_\Phi^{t}_{k} \longleftarrow \Phi^{t+1}_{k}$
13: $temp\_\Psi^{t}_{k} \longleftarrow \Psi^{t+1}_{k}$
14: $t \longleftarrow t+1$
15: **goto** *Step 4.*
16: **Extract common object(s)**: The location with $\Phi^{t+1}_{k} = \Psi^{t+1}_{k} > 0$ are common object(s) pixels for I_k.

The outer contour has been set up with a grant that $f[I_k(x,y), r_{\Phi}(C^{i}_{1-k})] > f[I_k(x,y), r_{\Phi}(C^{o}_{k})]$. Similarly, the inner contour has been set up with a grant that $f[I_k(x,y), r_{\Psi}(C^{i}_{1-k})] < f[I_k(x,y), r_{\Psi}(C^{o}_{k})]$. But, as the method is related to energy minimization problem, so as a consequence, with the increase in number of iterations t, for outer contour $f[I_k(x,y), r_{\Phi}(C^{i}_{1-k})] < f[I_k(x,y), r_{\Phi}(C^{o}_{k})]$ and for inner contour $f[I_k(x,y), r_{\Psi}(C^{i}_{1-k})] > f[I_k(x,y), r_{\Psi}(C^{o}_{k})]$. This in turn, will result in the minimization of the energy function, later this will results in the accurate separation of the common object(s) from the images. Since, the introduced method is based upon the work of Meng et al. in [15], so for measurement of similarity, reward strategy has been implemented. The related outcome is that, for given images if few pixels are similar to the background in the other image, and on the same side the background with uniform color distribution occupies a large region of one image, a pixel of background with massive background reward $f[I_k(x,y), r_{\Phi}(C^{o}_{k})]$ will also have a large foreground reward $f[I_k(x,y), r_{\Phi}(C^{i}_{1-k})]$ [15]. With the increase in iterations when foreground reward is lesser than background award, the pixel will be considered to belong to the background region, i.e., $f[I_k(x,y), r_{\Phi}(C^{i}_{1-k})] < f[I_k(x,y), r_{\Phi}(C^{o}_{k})]$ [15]. In the similar way, the opposite holds true for the case of inner contour. This in turn will help in the improvement of the co-segmentation output. However, SACM based co-segmentation only with outer or inner contour cannot extract out the common object(s) with increased accuracy label. This is due to the mentioned limitation of SACM. As such both the contour formulations (Eqs. (10) and (11)) have been coupled with each other along with $\tau \int_{\Omega}[H(\Phi(x,y)) - H(\Psi(x,y))]^2$, in order to benefit each other synergistically and to generate more improved co-segmentation output. Inherently, the term $\tau \int_{\Omega}[H(\Phi(x,y)) - H(\Psi(x,y))]^2$ act as an extra force to overcome the limitation of SACM, and allow the contours to reach at global minima. The consequence of the term has been discussed in details, in Section 4.6.

The main advantage of the proposed DGACM based co-segmentation is that, the method is not limited to the problem of stucking to local minima like SACM. Side-by-side, the formulation has also overcome the limitation due to inability of information sharing like classical DGACM based segmentation. Basically, the proposed formulation has incorporated the advantages of SACM based co-segmentation and DGACM based segmentation formulations, and draw out their limitation. That is, in the proposed formulation, both the formulations (DGACM based segmentation and SACM based co-segmentation) benefit each other collectively. Here lies the main novelty of the proposed method. Thus, the proposed model is capable of overcoming the problem of misclassification. Moreover the proposed method does not depend on the accurate prior information of the object for successful seg-

Fig. 3. Different initial inner contour set-up for co-segmentation.

mentation like MRF model for co-segmentation [3,13,11]. Beside the mentioned advantages, the proposed method is also capable of overcoming the drawback of clustering based co-segmentation. That is, the method does not need the assumption that the foreground and background intensity should differ highly.

3.3. Contour initialization

Technique for initializing the inner contours in different positions of the input image set has also been experimented in the proposed work. By nature, the success of contour based image analysis depends on initialization of the contours. In the proposed work contours have been initialized under four necessary conditions. These are:

- Two contours should be initialized in such a way that $E^{*}_{coseg}(\Phi) > E^{*}_{coseg}(\Psi)$.
- The terms $f[I_k(x,y), r_{\Phi}(C^{i}_{1-k})]$ and $f[I_k(x,y), r_{\Psi}(C^{i}_{1-k})]$ should always be *greater than* 0.
- For initial outer contour $f[I_k(x,y), r_{\Phi}(C^{i}_{1-k})] > f[I_k(x,y), r_{\Phi}(C^{o}_{k})]$.
- For initial inner contour $f[I_k(x,y), r_{\Psi}(C^{i}_{1-k})] < f[I_k(x,y), r_{\Psi}(C^{o}_{k})]$.

The outer contours for all the images have been initialized near the boundary of the images in such a way that the contour can circumscribe (enclose) the object region, so that it can have enough foreground information. The inner curve has been placed at three different positions heuristically. The work has been carried out by placing the initial inner contours **(a)** inside the common objects in the images, **(b)** outside the common objects and **(c)** randomly near the centre pixels of the images, respectively. Different initial inner contour positions are shown in Fig. 3.

From the contour set-up as shown in Fig. 3, it can be stated that, both the initial inner contour set-up inside the common objects boundary and near the centre pixels of the images, should produce similar outputs. On the other hand, initial inner contour set-up outside the common objects may provide improper results. This is due to the fact that initial inner contour outside the common objects does not have any information about the objects and as such process may get terminated quickly without generating the proper pixel information inside the inner contours. On the other hand initial inner contour set-up inside the boundary of the common objects and randomly near the center pixels of the images, both share information about the objects in the images and as a result both the set-up are supposed to generate better output as compared to the inner contour set-up outside the common object(s) boundary. In case of initial inner contour set-up inside the boundary of the common objects as stated by Gunn and Nixon [18] and Zhu et al. [19], respectively, for single image segmentation, the problem becomes fully supervised, i.e. it requires user interaction to set-up the initial inner contour inside the boundary of the common objects. In contrast, the proposed method chooses the initial inner contour randomly near the center pixels of the images so that the common object(s) detection problem can be carried out automatically without any human interaction. The main advantage of the proposed method for co-segmentation is that, it can handle information from both the contours present in the images. Thus it can gather more data about the common pixels present in the images. This will result in less misclassification of the regions present in the images and hence will increases the accuracy. Visual as well as quantitative analysis based on the contour initialization has been discussed in Section 4.5.

4. Results and discussion

4.1. Visual analysis

Experiments are conducted on 20 pairs of images, each image pair containing a common object(s) (the used pairs of images are given in supplementary file). The data set has been collected from Caltech-256 Object Categories database[1] and Microsoft Research Cambridge image database.[2] For the experiment, two contours are automatically initialized in each image. The initial outer contours are set up near the boundary of the images, which are made to shrink towards the common object(s) boundary and initial inner contours are set near the centre of the images. For the experiment $\lambda^{i}_{\Phi k} = \lambda^{o}_{\Phi k} = \lambda^{i}_{\Psi k} = \lambda^{o}_{\Psi k} \geq 1$ have been kept for all considered contours based models. The term τ is varied according to the complexity present in the images. Number of iterations for the experiment are also varied according to the size and complexity of the images. The maximum image size used in this experiment is 128×128 pixels.

A comparison between the results obtained using C-VACM (3rd row) and DGACM (4th row) of segmentation, and unsupervised learning model (USL) (5th row), MRF model (6th row), Co-fusion model (7th row), co-skeletonization (Co-skele) model (8th row), SACM of co-segmentation (9th row) and the proposed DGACM of co-segmentation (last row) along with the original images (OI) (1st row) and ground-truth (GT) images (2nd row) are visually shown in Figs. 4 and 5 (more results can be found in supplementary file). While comparing the outcome of the proposed method with the existing methods of co-segmentation using SACM, it has been found that the proposed method of co-segmentation is capable of extracting out common objects more accurately.

From Fig. 4a(i), containing the image of *pvoctraind*, it can be seen that in the ninth row the outcomes of co-segmentation using SAC, the green region (actually background) has been misclassified as the foreground region. Whereas, the outcome of the proposed model (given in the last row of the columns) shows that the method is able to extract actual foreground regions of images. Therefore, it increases the overall accuracy of co-segmentation. But for both the output images (corresponding image of *pvoctraind* shown in the ninth and tenth row of Fig. 4a(ii)), the *lamp post* has been misclassified as the foreground object. This is due to the fact that the algorithm is based on the reward strategy, i.e. the pixels will be rewarded if it has the same intensity as the foreground pixels of the other image. In this case, the *lamp post* and the *railway-engine* have

[1] http://www.vision.caltech.edu/Image_Datasets/Caltech256/.
[2] http://research-srv.microsoft.com/en-us/downloads/b94de342-60dc-45d0-830b-9f6eff91b301/default.aspx.

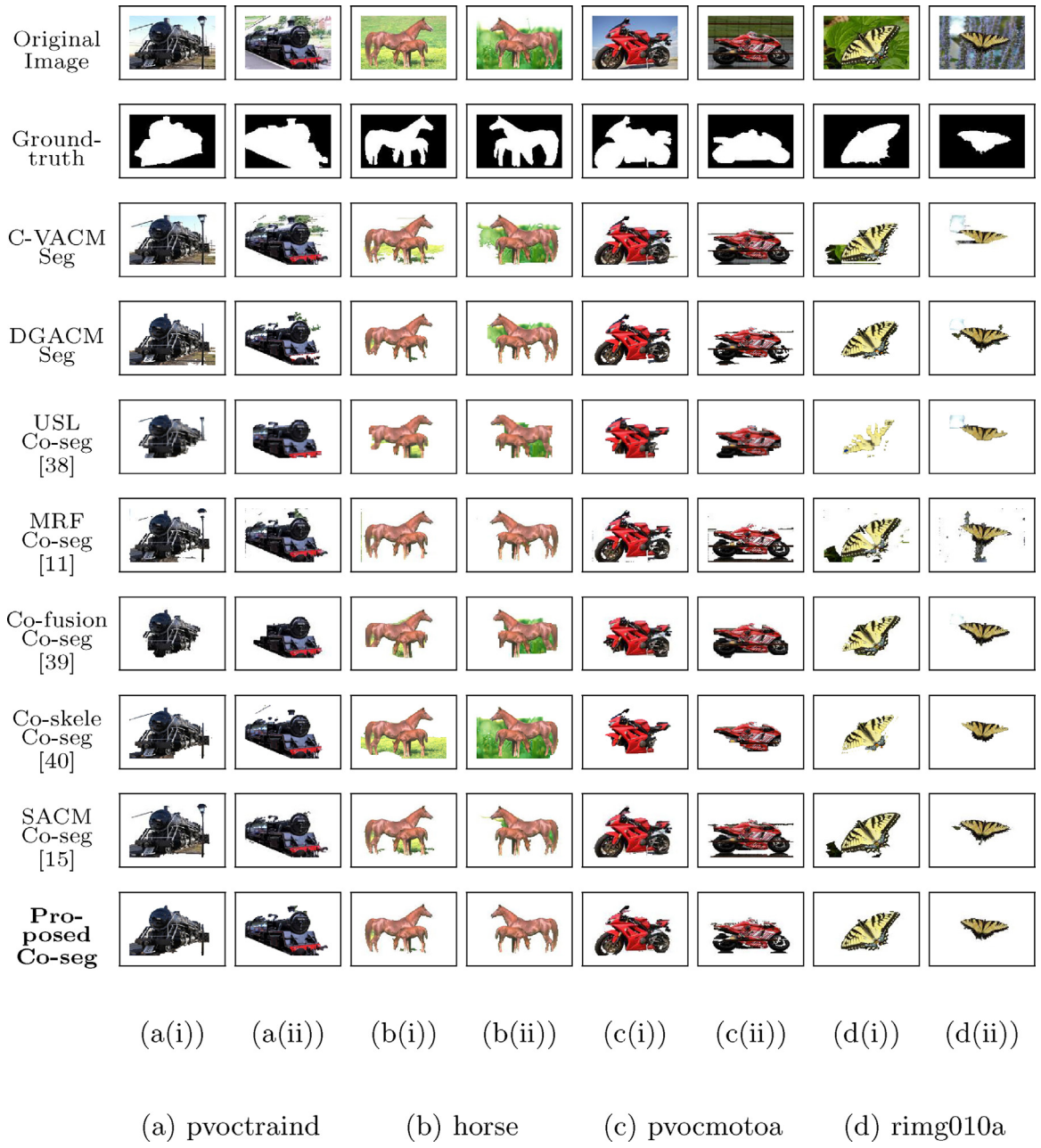

Fig. 4. A pictorial summarization of comparative studies between existing algorithms and the proposed method.

the same color. Similarly, in case of *horses* image, shown in Fig. 4b(i) and (ii), the single contour co-segmentation results shown in the ninth row has misclassified the green region as the foreground object. But co-segmentation using the proposed method is able to overcome this misclassification and can detect only the *horses* as the common object. Now the results of the *rimg010a* shown in the last two columns of Fig. 4, can be seen that both the output shown in the third and ninth rows of the mentioned column have detected the region apart from *butterfly* as the foreground region. This is due to the fact that the SAC searches the local minima present in the image, and by virtue of this, it gets stuck to the border of the black region where it detects the local minima.

In Figs. 4c and 5c containing the images of a *pvocmotoa* and a *rimg064a*, respectively, it can be seen that the original images shown in the first row of the figures contain some shadow portion. Output of co-segmentation using the SAC is unable to remove the shadow region from common object regions and as a result, accuracy of common object(s) detection becomes less as compared to it using the proposed method. The proposed method overcomes the drawback of SACM (see Figs. 4(ii) and 5c(ii)). This is because, while performing co-segmentation, it is incorporating information of the color intensity of the corresponding images from the two contours (inner and outer). The outer contour, while shrinking towards the common object(s) boundary, gets stuck to the boundary of the shadowed region due to the property of the SAC, because near the boundary it finds the strong edges compared to other portions of the images. This is due to the fact that the single contour is incorporating information about the pixels from one-side (inward information). On the other hand, in case of dual contours, one contour shrinks towards the object boundary and other contour expands towards the object boundary. As a result the dual contour is gathering information from both the contours. This in turn causes the two contours attract each other. Force of the inner contour pull the outer contour toward itself, thus avoiding the outer contour to

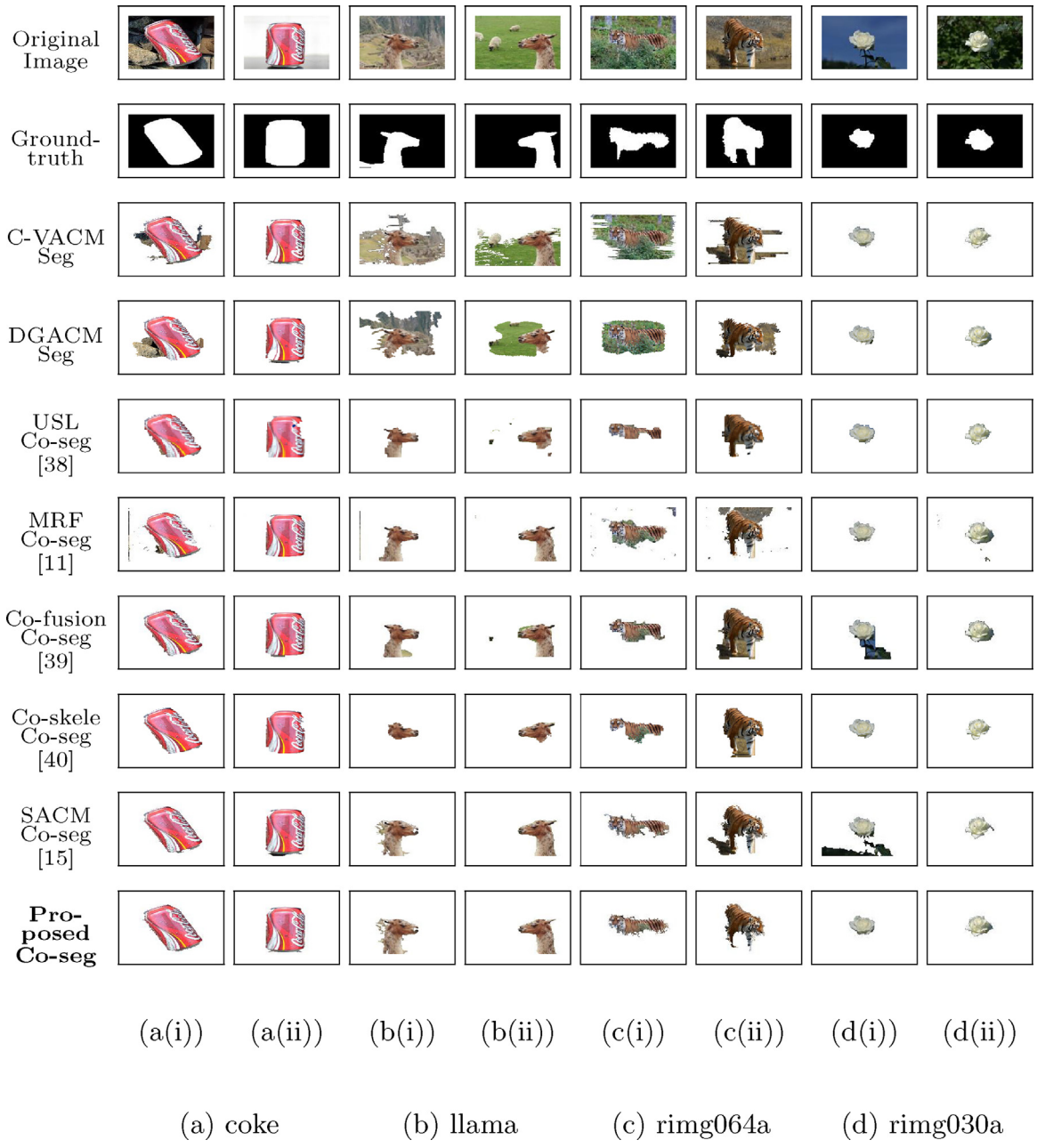

Fig. 5. A pictorial summarization of comparative studies between existing algorithms and the proposed method.

stuck to local minima. As a result the proposed method succeeds in eliminating the shadowed region while co-segmenting the images.

Similar to the results discussed above, the proposed method produces better results for all the image pairs, except *llama* image. The co-segmentation using SACM provide better results for *llama* image than the proposed method. This is due to the fact that in the second image of *llama* shown in Fig. 5b(ii) near the neck portion of *llama* image has been over segmented.

4.2. Quantitative analysis

Accuracy of the proposed algorithm has been compared based on the error-rate calculated from eight output, i.e., output of segmentation using SAC and DGAC, co-segmentation using USL, MRF, Co-fusion, Co-skele, SAC and co-segmentation using the proposed method. The error-rate of the segmented output has been calculated by taking the ground-truth. It is the ratio of the number of misclassified pixels to the total number of pixels present in the images. The ground-truths/segmentations are available in [15]. The error-rate of co-segmentation using the DGACM, the SACM, Co-fusion model, Co-skele model, MRF model, unsupervised learning model, segmentation using SACM and DGACM are given in Table 1 (error-rate table for the rest of the dataset are given in supplementary file). From this table it can be seen that for most of the images, the DGACM produces a lower error-rate as compared to the SACM. This is due to the global searching nature of DACM. The proposed method has a higher error-rate to *llama* image as compared to SACM of co-segmentation, due to the visual indifference mentioned earlier.

The result has also been tested with a few segmentation evaluation metrics like: Probabilistic Rand Index (PRI), Variation of Information (VI) and Global Consistency Error (GCE). For the purpose, each of the results is compared with its corresponding ground-truth image. The average value for each pair of images is

Table 1
Error-rate of segmentation using C-VACM, DGACM, co-segmentation using USL [38], MRF [11], Co-fusion [39], Co-skele [40], ACM [15], and the proposed method.

Methods compared	Image name							
	Pvoctraind	Horse	Pvocmotoa	Rimg010a	Coke	Llama	Rimg064a	Rimg030a
Segmentation using C-VACM	0.1990	0.1753	0.0839	0.1138	0.0828	0.4023	0.3198	0.0118
Segmentation using DGACM	0.1537	0.0963	0.0722	0.0524	0.0840	0.3952	0.2195	0.0086
Co-segmentation using USL [38]	0.1190	0.1338	0.1580	0.1531	0.0786	0.0890	0.1061	0.0518
Co-segmentation using MRF [11]	0.1019	0.0505	0.1011	0.0926	0.0495	0.0359	0.1093	**0.0059**
Co-segmentation using co-fusion [39]	0.1295	0.1015	0.0773	0.0446	**0.0183**	0.0567	0.0789	0.0539
Co-segmentation using co-skele [40]	0.0719	0.2903	0.1757	0.0653	0.0315	0.1077	0.0762	0.0122
Co-segmentation using ACM [15]	0.1034	0.0599	0.0661	0.0321	0.0204	**0.0349**	0.0656	0.0690
Co-segmentation using proposed method (DGACM)	**0.0690**	**0.0493**	**0.0602**	**0.0219**	**0.0183**	0.0360	**0.0568**	0.0087

Table 2
Evaluation metrics of segmentation using C-VACM, DGACM, co-segmentation using USL [38], MRF [11], Co-fusion [39], Co-skele [40], ACM [15], and the proposed method.

Methods compared	Segmentation matrics	Image name							
		Pvoctraind	Horse	Pvocmotoa	Rimg010a	Coke	Llama	Rimg064a	Rimg030a
Segmentation using C-VACM	PRI	0.6920	0.7168	0.8465	0.7983	0.8483	0.5253	0.6048	0.9767
	VI	1.1350	1.1290	0.7854	0.9305	0.6940	1.4558	1.2887	0.1396
	GCE	0.2383	0.2464	0.1472	0.1810	0.1346	0.2687	0.2544	0.0195
Segmentation using DGACM	PRI	0.7487	0.8352	0.8723	0.9051	0.8511	0.5275	0.6613	0.9859
	VI	1.0829	0.8173	0.7008	0.4824	0.7302	1.6348	1.2772	0.1041
	GCE	0.2282	0.1584	0.1259	0.0813	0.1382	0.2983	0.2472	0.0134
Co-segmentation using USL	PRI	0.7905	0.7690	0.7394	0.7440	0.8552	0.8379	0.8110	0.9021
	VI	1.0017	1.1132	1.1379	1.0567	0.7530	0.7399	0.8960	0.4542
	GCE	0.2020	0.2266	0.2364	0.1958	0.1367	0.1259	0.1653	0.0701
Co-segmentation using MRF	PRI	0.8198	0.9042	0.8211	0.8326	0.9064	0.9314	0.8080	**0.9884**
	VI	0.8946	0.5224	0.9057	0.8225	0.5202	**0.3662**	0.9088	**0.0884**
	GCE	0.1751	0.0903	0.1761	0.1521	0.0900	**0.0589**	0.1709	**0.0111**
Co-segmentation using co-fusion	PRI	0.7765	0.8193	0.8623	0.9147	0.9640	0.8936	0.8555	0.9024
	VI	0.8897	0.9198	0.6644	0.4618	0.2446	0.5481	0.6682	0.3669
	GCE	0.1920	0.1771	0.1280	0.0766	0.0353	0.0909	0.1219	0.0486
Co-segmentation using co-skele	PRI	0.8671	0.5948	0.7129	0.8800	0.9393	0.8087	0.8595	0.9760
	VI	0.6743	1.3345	1.0776	0.5180	0.3431	0.6654	0.6991	0.1402
	GCE	0.1272	0.3011	0.2264	0.0936	0.0572	0.0912	0.1203	0.0196
Co-segmentation using ACM	PRI	0.8189	0.8874	0.8779	0.9384	0.9601	**0.9342**	0.8779	0.8769
	VI	0.8250	0.6298	0.6288	0.3516	0.2722	0.3703	0.6531	0.4558
	GCE	0.1667	0.1092	0.1149	0.0577	0.0394	0.0623	0.1130	0.0597
Co-segmentation using proposed method (DGACM)	PRI	**0.8726**	**0.9064**	**0.8868**	**0.9573**	**0.9642**	0.9314	**0.8932**	0.9828
	VI	**0.6632**	**0.4987**	**0.6285**	**0.2537**	**0.2357**	0.3884	**0.5384**	0.1179
	GCE	**0.1228**	**0.0871**	**0.1108**	**0.0399**	**0.0347**	0.0647	**0.0900**	0.0158

taken as the final output value for each of the metrics. It is expected that if PRI is having a higher value, and VI and GCE have a lower value, then the generated output is better. From the results shown in Table 2, it can be stated that the results obtained from the proposed method are well acceptable with the expectation for most of the images.

4.3. *Dual contour based co-segmentation vs. dual contour based segmentation*

From the output given in the third and fourth rows of Figs. 4 and 5 and results given in Table 1, it can be concluded that the DGACM based segmentation is capable of detecting the accurate boundary in the image as compared to the C-VACM. But the pixels located inside the boundary detected by DGACM based segmentation cannot be considered as the pixels of the common object(s). Here lies the main difference between image segmentation using DGACM and image co-segmentation using DGACM. Co-segmentation using DGACM is capable of detecting the accurate common object(s) boundary, where the region inside the boundary can be considered as the common object(s) present in the given images. From the images shown in the third and fourth rows of Fig. 5c and Table 1, it can be concluded that DGACM based segmentation method has detected the boundary of the object accurately compared to C-VACM. But, the main problem associated with DGACM based image segmentation is that, they are unable to hold the semantic information about the object(s) present in the image. As a result, some portions of the object(s) are detected as background and vice-versa. On the other hand, the DGACM based image co-segmentation is able to hold the semantic information about the common object(s) present in the images and thus it is able to extract out the exact object(s) present in the images.

Moreover, DGACM based image segmentation is associated with detecting and extracting out the various homogeneous regions present in a single image. In contrast, the proposed DGACM formulation for co-segmentation focuses only on extraction of the common object(s) associated with the given images.

In short it can be stated that, DGACM based image segmentation [19,20] technique had been developed for single image segmentation only, with a motivation to partition an image into distinct regions having similar attributes. On the other hand DGACM for co-segmentation has been proposed with a motivation to extract out the common object(s) from the images, where the number of images is generally $\geq$2. In addition, the terms related to pixels information sharing is absent in the formulation of DGACM based image

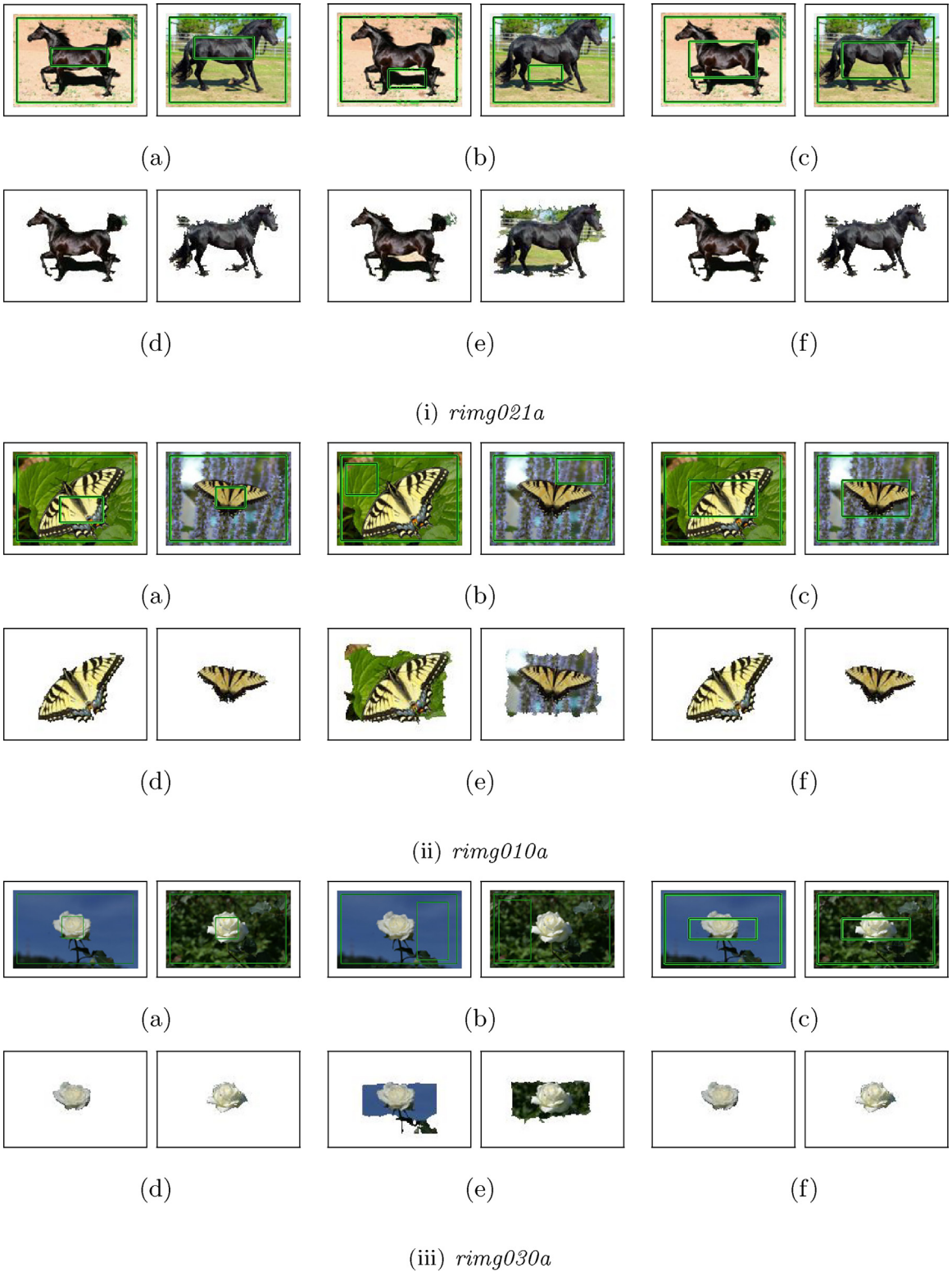

Fig. 6. First row in (i)–(iii) shows the initial inner contour set-up for co-segmentation and the second one shows the corresponding output for different inner contour set-up.

segmentation as already stated in Section 3.2, unlike DGACM based co-segmentation.

4.4. Computational time required

From the experiments conducted, it can be claimed that within 850 iterations, the proposed method is capable of extracting the common object(s) with higher accuracy for any size of images used in the experiment. Alongside, based on Figs. 4 and 5, and Table 1, it is observed that the proposed method provides better results with less number of iterations as compared to SACM based co-segmentation.

The time required to generate the output by the proposed method is high in most of the cases compared to the SACM. This

Table 3
Error-rate of co-segmentation using the proposed method for different inner contour positions.

Inner contour position	Image name					
	Banana	Coke	Pvoctraind	Rimg010a	Rimg021a	Rimg030a
Inside the object	**0.0303**	**0.0182**	0.0814	0.0225	**0.0533**	0.0090
Outside the object	0.2857	0.2460	0.1616	0.2911	0.1514	0.1988
Random	**0.0303**	0.0183	**0.0690**	**0.0219**	**0.0533**	**0.0087**

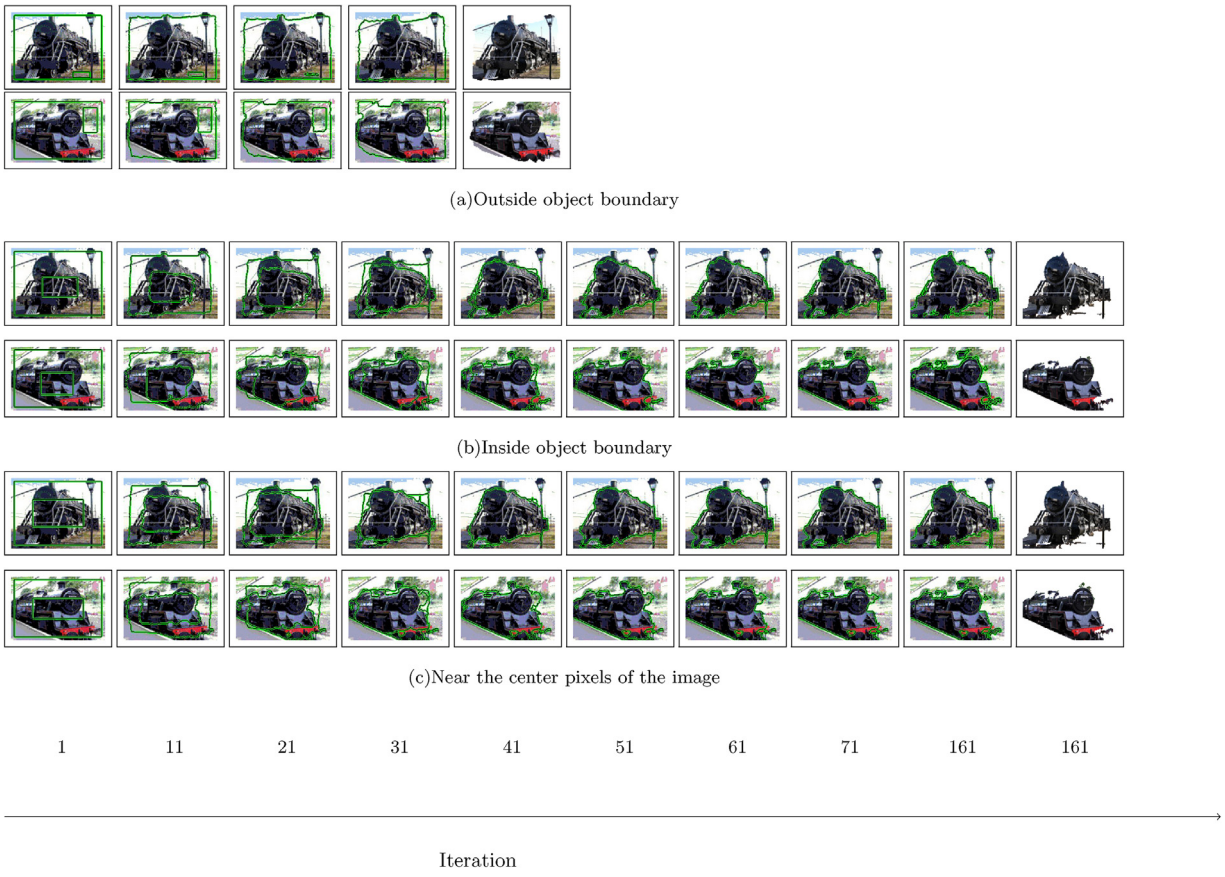

Fig. 7. Figures (a)–(c) shows how the inner contour evolves at each iteration for different initializations and the last image in each row shows the corresponding output for different inner contour set-up. The work has been carried out using ***pvoctraind*** image set for τ value at 0.2.

is due to the fact that in case of dual active contours, the algorithm is extracting information from both the contours, inner and outer separately while SACM extracts information from the outer or the single contour only. But if the size of the images is relatively small and the difference between the number of iterations required in the two methods is large (exceeding 650 or above), the proposed method takes less time to generate the output.

4.5. Results for different contour initialization

For the same input images, different positions are chosen to set-up the initial inner contour, and the corresponding outputs are shown in Fig. 6 (more results and the error-rate graph for the corresponding results are shown in the supplementary file). As stated earlier in Section 3.3, the work has been carried out by placing the initial inner contour **(a)** inside the common objects, **(b)** outside the common objects and **(c)** randomly chosen at a place near the centre pixels of the images, respectively.

Pixel error-rates obtained using the proposed method for different positions of initial inner contours are summarized in Table 3. The output suggests that the error-rate is higher for case (b), whereas case (a) and (c) produce similar (with approximate equal error-rate) and better results. This is possible because, both (a) and (c) take the information about the common objects in the images. Contour evolution for different inner contour initialization and the corresponding outputs are shown in Fig. 7.

Since the object is located near the centre of the images, initialization of the inner contours as stated in case *(c)* gets better common foreground pixels information and extracts common objects automatically with higher accuracy. This is a limitation of the proposed method as the object could as well be located in different regions of the image (not necessarily near the center of the images). In such cases, the inner contour may fail to converge to the boundary of the common object(s).

4.6. Discussion

Co-segmentation results using the proposed method mainly depend on five parameters, namely $\lambda^{i}_{\Phi k}$, $\lambda^{o}_{\Phi k}$, $\lambda^{i}_{\Psi k}$, $\lambda^{o}_{\Psi k}$, and τ. From the mathematical expressions given in Eqs. (22) and (23), it can be portrayed that the terms $[H(\Phi(x, y)) - H(\Psi(x, y))]$ and $[H(\Psi(x, y)) - H(\Phi(x, y))]$ add zero influence for the pixels outside both the inner and outer contours or the pixels inside both inner and outer

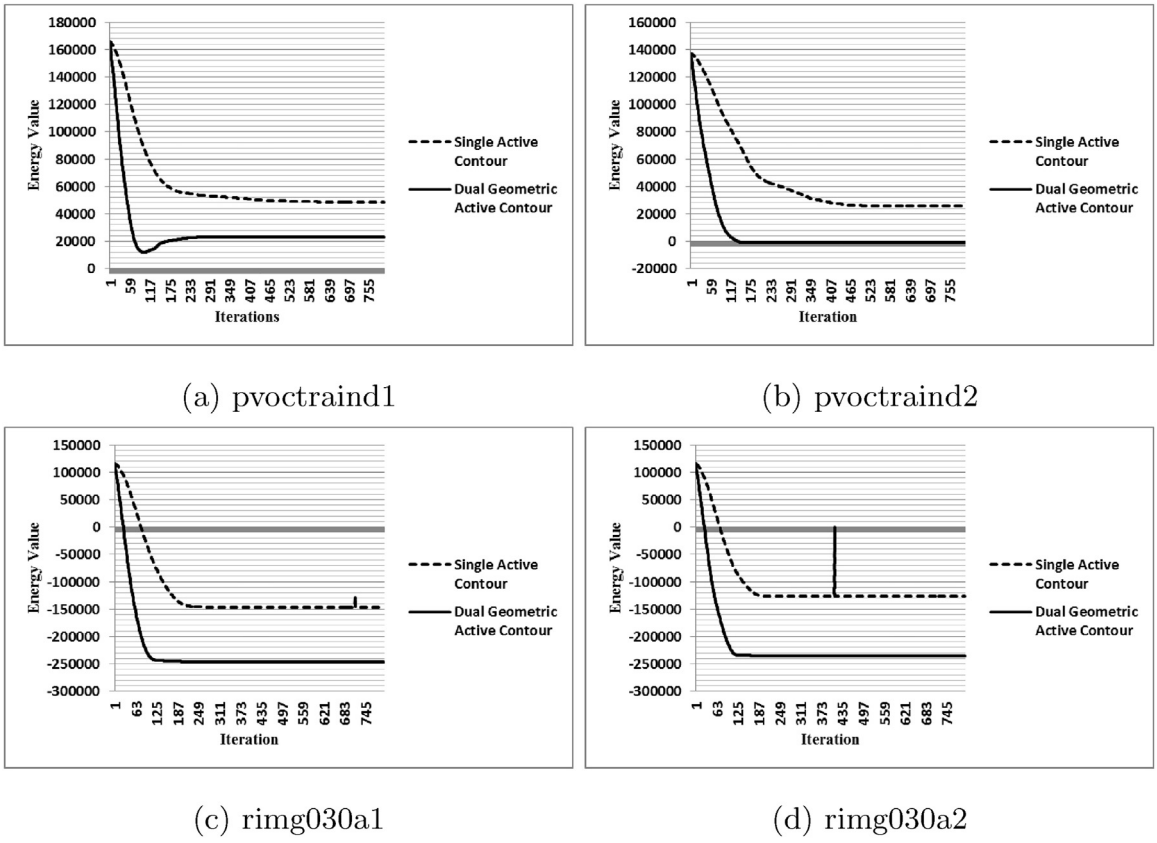

Fig. 8. Graph representing total energy value of outer contour for different images.

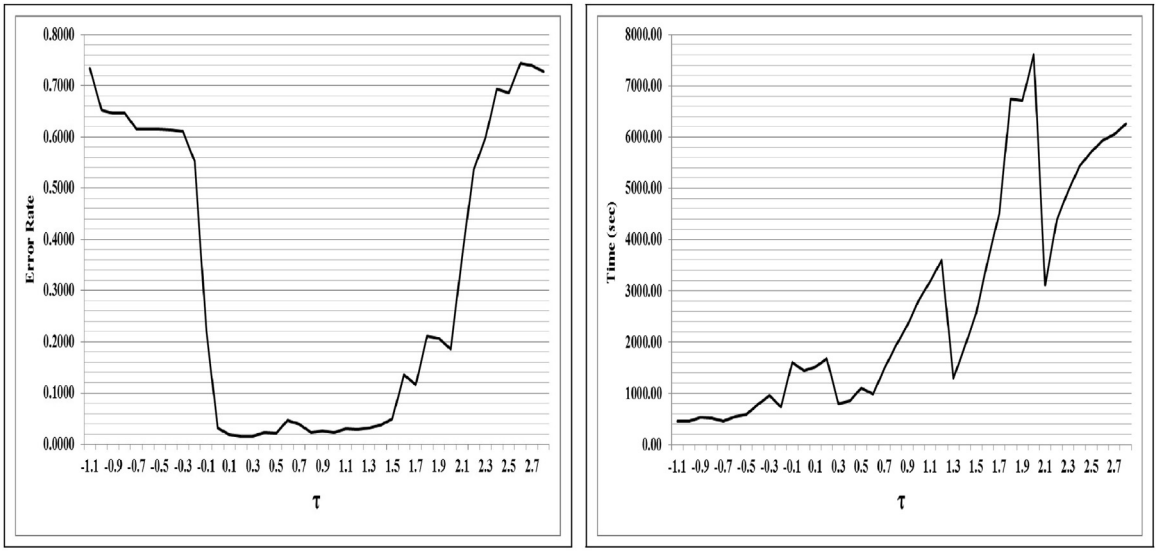

Fig. 9. First row shows the error-rate vs τ plot and the second row shows the time vs τ plot for rimg010a images for the proposed model.

contours (as the terms $H(\Phi(x, y))$ and $H(\Psi(x, y))$ cancel each other). The term exists if and only if $H(\Phi(x, y))$ is not equal to $H(\Psi(x, y))$ and either $H(\Phi(x, y))$ or $H(\Psi(x, y))$ has unit value. This is only possible if the pixels are present between outer and inner contours, where $H(\Phi(x, y))$ is equal to 1 and $H(\Psi(x, y))$ is 0. Overall, it can be concluded that the term $[H(\Phi(x, y)) - H(\Psi(x, y))]$ adds a negative effect to the energy of the outer contour and as a result it moves the contour towards the common object(s) boundary. While the term $[H(\Psi(x, y)) - H(\Phi(x, y))]$ adds a positive effect on the inner contour to expand it towards the common object(s) boundary. Thus, it can be concluded easily, that adding extra contour with the existing SACM will provide extra force. The graphs shown in Fig. 8 validates the effect of extra contour (inner contour). The graph indicates how the energy value of the outer contour gets minimized by the pro-

posed DGACM based co-segmentation as compared to SACM, with increase in iterations.

The parameter τ determines how rapidly the two contours (inner and outer) converge with each other. If τ is negative, it produces the inverse effect on these terms and as a result, the outer contour will expand towards the boundary of the image and the inner contour will shrink towards the center of the image, which is contrary to the objective of the work. Thus, in the experiment, τ is taken positive. On the other hand a higher value of τ will force the outer contour to cross out the inner contour and shrink towards the center of the image and the inner contour will move towards the image boundary, which is also contrary to the objective of the proposed work. Experimentally, it has been observed from the graphs given in Fig. 9 (more graph can be found in supplementary file), the error-rate of the proposed method increases if the value of τ is less than 0 or above 1. It has been noticed from the graphs, that the proposed method is generating better results and take less time for $\tau \in (0, 1]$. So in the present work, τ value is kept in the half-closed interval $(0, 1]$. It has been observed that the two contours get merged quickly if τ is increased in $(0, 1]$. Based on the complexity of the images the parameter τ has been tuned.

The parameters $\lambda^i_{\Phi k}$ and $\lambda^i_{\Psi k}$ control the common foreground consistency inside the inner and the outer contours respectively. The method is able to detect more similar region(s) of the common object(s) with the increment of the weight of these parameters. As a result the rate of misclassification gets reduced. On the other hand, decrement of these parameters values eliminates most of the common parts in the images. That is, the common foreground part(s) is detected as the background, resulting in improper segmentation result. Similarly, the decrement of the weight of $\lambda^o_{\Phi k}$ and $\lambda^o_{\Psi k}$, reduces the background consistency, and as a result the background region in the images is detected as foreground region. It also enhances the misclassification rate while detecting the co-occurrence of the object(s) in the images.

5. Conclusion

In this article, the task of co-segmentation to extract common object(s) from given images has been performed using DGACM. The method overcomes the problem of contour attraction towards local minima, associated with the single contour method. Thus, it reduces the misclassification of pixels. The method searches global minima without human interactions, especially for images having objects near the centre of the images. Empirical results manifest that the proposed model for co-segmentation expel out the common object(s) from the images with lower error-rates as compared to other algorithms involved in the field of co-segmentation. Based on the experimental results, it can also be stated, that the proposed method gives better results for images with shadows. That is, DGACM based co-segmentation is capable of detecting only the common object(s) by eliminating shadows in the images. It can be claimed that the proposed method gives better accuracy in detecting the objects present in the images, compared to the single image segmentation results. However, the time required for co-segmenting the images by the proposed model is more in most of the cases as compared to the other existing algorithms. It is because the DGACM is gathering information from both the contours. But, if the size of the images is small and the difference between the number of iterations required by ACM for co-segmentation and the proposed model is quite large, then the time required to generate the result by the proposed method is quite less. In future, the accuracy of co-segmentation result will be tried to increase by incorporating other image features, mainly for the images containing object(s) with complex background. The limitation of inner contour initialization also needs to be resolved in a future work such that the method automatically extracts the common objects located away from the centre of the images, independent of any human interaction.

Appendix A. Supplementary data

Supplementary data associated with this article can be found, in the online version, at https://doi.org/10.1016/j.asoc.2018.02.034.

References

[1] D.-J. Chen, H.-T. Chen, L.-W. Chang, Video object cosegmentation, 20th ACM International Conference on Multimedia (2012) 805–808.
[2] D. Zhang, O. Javed, M. Shah, Video object co-segmentation by regulated maximum weight cliques, in: Computer Vision – ECCV 2014, Springer International Publishing, 2014, pp. 551–566.
[3] C. Rother, T. Minka, A. Blake, V. Kolmogorov, Cosegmentation of image pairs by histogram matching – incorporating a global constraint into MRFs, IEEE Computer Society Conference on Computer Vision and Pattern Recognition, vol. 1 (2006) 993–1000.
[4] S. Vicente, C. Rother, V. Kolmogorov, Object cosegmentation, IEEE Conference on Computer Vision and Pattern Recognition (2011) 2217–2224.
[5] G.W. Jiji, P.J. DuraiRaj, Content-based image retrieval techniques for the analysis of dermatological lesions using particle swarm optimization technique, Appl. Soft Comput. 30 (2015) 650–662.
[6] M. ElAlami, A new matching strategy for content based image retrieval system, Appl. Soft Comput. 14 (Part C) (2014) 407–418.
[7] J. Cui, Q. Yang, F. Wen, Q. Wu, C. Zhang, L. Van Gool, X. Tang, Transductive object cutout, IEEE Conference on Computer Vision and Pattern Recognition (2008) 1–8.
[8] S. Vicente, V. Kolmogorov, C. Rother, Cosegmentation revisited: models and optimization, 11th European Conference on Computer Vision (2010) 465–479.
[9] A. Gallagher, T.C.T. Chen, Clothing cosegmentation for recognizing people, IEEE Conference on Computer Vision and Pattern Recognition (2008) 1–8.
[10] K. Cai, W. Shao, X. Yin, G. Liu, Co-segmentation of aircrafts from high-resolution satellite images, 11th IEEE International Conference on Signal Processing (2012) 993–996.
[11] D. Hochbaum, V. Singh, An efficient algorithm for co-segmentation, IEEE 12th International Conference on Computer Vision (2009) 269–276.
[12] G. Tsechpenakis, R.E. Gamage, M.D. Kim, A. Chiba, Motor neuron morphology estimation for its classification in the Drosophila brain, 33rd Annual International Conference of the IEEE Engineering in Medicine and Biology Society (2011) 7755–7758.
[13] L. Mukherjee, V. Singh, C. Dyer, Half-integrality based algorithms for cosegmentation of images, in: 2009 IEEE Conference on Computer Vision and Pattern Recognition, Miami, FL, 2009, pp. 2028–2035.
[14] S.T. Gollmer, M. Simon, A. Bischof, J. Barkhausen, T.M. Buzug, Multi-object active shape model construction for abdomen segmentation: preliminary results, 34th Annual International Conference of the IEEE Engineering in Medicine and Biology Society (2012) 3990–3993.
[15] F. Meng, H. Li, G. Liu, K.N. Ngan, Image cosegmentation by incorporating color reward strategy and active contour model, IEEE Trans. Syst. Man Cybern. Part B (Cybern.) 43 (2) (2013) 725–737 http://ivipc.uestc.edu.cn/project/FanmanMeng_SMCB/.
[16] T.F. Chan, L.A. Vese, Active contours without edges, IEEE Trans. Image Process. 10 (2) (2001) 266–277.
[17] S. Liu, Y. Peng, A local region-based Chan–Vese model for image segmentation, Pattern Recognit. 45 (7) (2012) 2769–2779.
[18] S. Gunn, M. Nixon, A model based dual active contour, British Machine Vision Conference (1994) 305–314.
[19] G. Zhu, Q. Zeng, C. Wang, Dual geometric active contour for image segmentation, Opt. Eng. Lett. 45 (8) (2006) 1–3.
[20] X. Huang, H. Bai, S. Li, Automatic aerial image segmentation using a modified Chan–Vese algorithm, 9th IEEE Conference on Industrial Electronics and Applications (2014) 1091–1094.
[21] Y. Wu, W. Ma, M. Gong, H. Li, L. Jiao, Novel fuzzy active contour model with kernel metric for image segmentation, Appl. Soft Comput. 34 (2015) 301–311.
[22] S. Patra, R. Gautam, A. Singla, A novel context sensitive multilevel thresholding for image segmentation, Appl. Soft Comput. 23 (2014) 122–127.
[23] X.Y. Wang, W.W. Sun, Z.F. Wu, H.Y. Yang, Q.Y. Wang, Color image segmentation using PDTDFB domain hidden Markov tree model, Appl. Soft Comput. 29 (2015) 138–152.
[24] A. Mondal, S. Ghosh, A. Ghosh, Robust global and local fuzzy energy based active contour for image segmentation, Appl. Soft Comput. 47 (2016) 191–215.
[25] S.K. Pal, A. Ghosh, Image segmentation using fuzzy correlation, Inf. Sci. 62 (3) (1992) 223–250.
[26] Z. Gao, P. Shi, H.R. Karimi, Z. Pei, A mutual GrabCut method to solve co-segmentation, EURASIP J. Image Video Process. 2013 (20) (2013) 1–11.
[27] S. Geman, D. Geman, Stochastic relaxation, Gibbs distributions, and the Bayesian restoration of images, IEEE Trans. Pattern Anal. Mach. Intell. (6) (1984) 721–741.

[28] A. Ghosh, A. Mondal, S. Ghosh, Moving object detection using Markov random field and distributed differential evolution, Appl. Soft Comput. 15 (2014) 121–136.
[29] B.N. Subudhi, S. Ghosh, S.-B. Cho, A. Ghosh, Integration of fuzzy Markov random field and local information for separation of moving objects and shadows, Inf. Sci. 331 (2016) 15–31.
[30] Y.Y. Boykov, M.-P. Jolly, For optimal boundary & region segmentation of objects in N–D images, Eighth IEEE International Conference on Computer Vision (2001) 105–112.
[31] F. Meng, H. Li, K.N. Ngan, L. Zeng, Q. Wu, Feature adaptive co-segmentation by complexity awareness, IEEE Trans. Image Process. 22 (12) (2013) 4809–4824.
[32] H. Merdassi, W. Barhoumi, E. Zagrouba, Color images co-segmentation based on fuzzy local-entropy classification, Multimedia and Signal Processing (2012) 240–248.
[33] A. Joulin, F. Bach, J. Ponce, Discriminative clustering for image co-segmentation, 2010 IEEE Conference on Computer Vision and Pattern Recognition (2010) 1943–1950.
[34] B.-C. Lin, D.-J. Chen, L.-W. Chang, Unsupervised image co-segmentation based on cooperative game, in: 12th Asian Conference on Computer Vision, vol. 9005 of Lecture Notes in Computer Science, Springer International Publishing, 2014, pp. 51–63.
[35] A. Joulin, F. Bach, E.N. Sup, Multi-class cosegmentation, IEEE Conference on Computer Vision and Pattern Recognition (2012) 542–549.
[36] E. Kim, H. Li, X. Huang, A hierarchical image clustering cosegmentation framework, IEEE Computer Society Conference on Computer Vision and Pattern Recognition (2012) 686–693.
[37] A. Faktor, M. Irani, Co-segmentation by composition, IEEE International Conference on Computer Vision (2013) 1297–1304.
[38] J. Dai, Y.N. Wu, J. Zhou, S.-C. Zhu, Cosegmentation and cosketch by unsupervised learning, IEEE International Conference on Computer Vision (2013) 1305–1312.
[39] K.R. Jerripothula, J. Cai, J. Yuan, Image co-segmentation via saliency co-fusion, IEEE Trans. Multimed. 18 (9) (2016) 1896–1909.
[40] K.R. Jerripothula, J. Cai, J. Lu, J. Yuan, Object co-skeletonization with co-segmentation, IEEE Conference on Computer Vision and Pattern Recognition (2017) 3881–3889.
[41] K. Li, J. Zhang, W. Tao, Unsupervised co-segmentation for indefinite number of common foreground objects, IEEE Trans. Image Process. 25 (4) (2016) 1898–1909.
[42] W. Wang, J. Shen, Higher-order image co-segmentation, IEEE Trans. Multimed. 18 (6) (2016) 1011–1021.
[43] M.D. Collins, L. Grady, V. Singh, Random walks based multi-image segmentation: quasiconvexity results and GPU-based solutions, IEEE Conference on Computer Vision and Pattern Recognition (2012) 1656–1663.
[44] D. Batra, A. Kowdle, D. Parikh, J. Luo, T. Chen, iCoseg: interactive co-segmentation with intelligent scribble guidance, IEEE Conference on Computer Vision and Pattern Recognition (2010) 1–8.
[45] G. Kim, L. Fei-Fei, E.P. Xing, T. Kanade, Distributed cosegmentation via submodular optimization on anisotropic diffusion, International Conference on Computer Vision (2011).
[46] E.S. Brown, T.F. Chan, X. Bresson, Completely convex formulation of the Chan–Vese image segmentation model, Int. J. Comput. Vis. 98 (1) (2012) 103–121.
[47] G. Giraldi, P. Rodrigues, J. Suri, S. Singh, Dual active contour models for medical image segmentation, in: Image Segmentation, InTech, 2011.
[48] H. van der Pol, B. Bremmer, Operational Calculus Based on the Two-Sided Laplace Integral, Cambridge University Press, Cambridge, England, 1955.
[49] B. Dacorogna, Introduction to the Calculus of Variations, Imperial College Press, 2004.
[50] A. Mitiche, I. Ben Ayed, Variational and Level Set Methods in Image Segmentation, 5th ed., Springer-Verlag, Berlin Heidelberg, 2010.